Deliverable 2.1:
Historical trends in climate & water indicators over the Horn of Africa Drylands

Contributors:
David MacLeod (UoB), Dagmawi Asfaw (UoB), Katerina Michaelides (UoB), Akash Koppa (UGent), Jessica Keune (UGent), Diego G. Miralles (UGent), Michael Singer (CU)

Table of Contents

List of acronyms used in this report

AI - Aridity Index

ARC - African Rainfall Climatology

CHIRPS - Climate Hazards Group InfraRed Precipitation with Station data

CRU - Climate Research Unit

ECMWF - European Centre for Medium-Range Weather Forecasts

ENSO - El Niño-Southern Oscillation

ERA5 - ECMWF Reanalysis 5

FLEXPART - FLEXible PARTicle dispersion model

HAMSTER - Heat And MoiSture Tracking framEwoRk

GLEAM - Global Land Evaporation Amsterdam Model

GPCC - Global Precipitation Climatology Centre

GRACE - Gravity Recovery and Climate Experiment

HAD - Horn of Africa Drylands

IOD - Indian Ocean Dipole

MAM - March-April-May (long rains)

MSWEP - Multi-Source Weighted-Ensemble Precipitation

OND - October-November-December (short rains)

PET - Potential Evapotranspiration

SPEI - Standardized Precipitation Evapotranspiration Index

SPI - Standardized Precipitation Index

TWS - Total Water Storage

1 Motivation

The Horn of Africa drylands (HAD) encompass the majority of Kenya, Somalia and Ethiopia which experience an arid or semi-arid climate (Beck et al 2018). The region is regularly affected by extreme droughts (Haile et al 2020) and flooding (Kilavi et al 2018). This extreme climate variability leads to significant negative impacts on communities' lives and livelihoods across the region. To support adaptation to climate variability and enhance water security, the DOWN2EARTH project is co-designing a water information service to support community and individual decision making across the region.

To provide context to DOWN2EARTH activities, here we present an analysis of recent trends in climate and water indicators over the Horn of Africa drylands. In Section 2 we present a brief literature review. In Section 3 we describe DOWN2EARTH analysis focusing on climate trends. For rainfall: the spatial pattern of rainfall trends and trends in monthly rainfall, as well as trends in the contribution of extreme sub-daily rainfall to seasonal totals. We also present an analysis of the global sources of atmospheric water vapour to investigate relative changes in moisture contribution as a possible explanation for rainfall trends. Finally, an evaluation of potential evapotranspiration (PET) and aridity index over HAD is presented, based on a new dataset produced through DOWN2EARTH: hPET (Singer et al 2021).

Section 4 describes recent trends in water indicators which includes decadal trends in drought indices, an evaluation of annual and monthly soil moisture trends, and an estimation of trends in the availability of subsurface water. Finally, Section 5 provides a synthesis of the report, summarising understanding of rainfall and water-related trends over the Horn of Africa drylands.

Parts of the work presented here form the core of a DOWN2EARTH paper, currently in submission (Adloff et al., submitted). The full abstract of this paper is provided in an appendix. We also provide the abstract of Singer et al. (2021), describing the new hourly potential evapotranspiration dataset (hPET), and the abstract of Keune et al. (2021), which describes moisture tracking research which is discussed in this report.

2 Background

The Horn of Africa experiences two rainy seasons, as the tropical rain belt moves northward in boreal spring (March to May - MAM, hereafter the “long rains”), and returning southward in boreal autumn (October to December - OND, hereafter the “short rains”) (Nicholson, 2017). Compared to other locations in the tropics, annual rainfall totals in the region are low, due to suppressed convection via import of cool near-surface air from the Indian Ocean (Yang et al., 2015).

Since 2000, devastating droughts during the long rains (MAM) have increased in frequency in the region (Rowell et al., 2015). This has been attributed to anthropogenic warming of ocean temperatures in the Northwest Pacific, increasing the capacity of La Niña climate events in the Pacific to suppress the long rains (Funk et al., 2015). Despite this trend toward dry conditions, climate models consistently project wetter long rains. This apparent contradiction between observed and projected trends has been named the East African Climate Paradox (Rowell et al., 2015). Recent studies have suggested that the recent decline is associated with a shorter rainy season, with warmer waters south of East Africa driving later season onset and warming-driven lower surface pressure over Arabia leading to earlier cessation (Wainwright et al., 2019).

The short rains (OND) provide less total seasonal rain than the long rains on average (Nicholson 2017). However, year-to-year short rains variability is much higher due to the strong association with large-scale climate forcings such as the El Niño-Southern Oscillation, ENSO, and mediated by the Indian Ocean Dipole, IOD (MacLeod et al. 2020). Positive IOD events reverse the normal direction of atmospheric flow over the Indian Ocean, supporting significant enhancement of rainfall over the Horn of Africa. Notably in 2019 an extreme positive IOD occurred, leading to widespread death and destruction (Nicholson et al., 2021). This event was associated with an unprecedented basin-wide reversal of Indian Ocean temperatures, made possible through the anthropogenic climate warming trend (Funk 2021). Analysis of one observational rainfall dataset from 1981-2016 determined an increasing trend in short rains rainfall, although results did not indicate a statistically significant trend (Gebrechorkos et al., 2019).

In terms of temperature, the Horn of Africa has seen steady increases over the past fifty years, following the global trend (IPCC, 2021). Average daily maximum temperatures have increased at an average rate of 0.20 to 0.25ºC per decade, whilst daily minimum temperatures have increased at a rate of 0.17 to 0.22ºC per decade (Camberlin, 2017). Pan-Africa analysis has shown that this recent warming trend was accompanied by an increase in potential evapotranspiration (Onyutha, 2021).

3 Climate

3.1 Trends in rainfall

Rain gauges with continuous records spanning multiple decades are rare and sparse in the HAD. Trend assessment therefore relies on gridded data, originating from rain gauges, satellites, climate model reanalysis or methods which merge these sources. We describe the observational uncertainty in multi-decadal rainfall trends across HAD here, along with the spatial characteristics of trends. We use six commonly used rainfall datasets, representing the range of methods underlying gridded rainfall products. Details of the datasets used are provided in Table 1. We evaluated multi-decadal trends in monthly rainfall totals, in seasonal totals corresponding to the long rains and the short rains and in annual totals. Beyond these trends in rainfall totals, we extend analysis by using sub-daily data provided by MSWEP (Beck et al 2019) to estimate trends in the contribution of extreme rainfall to seasonal totals.

Gridded rainfall product	Data description	Reference
GPCC: Global Precipitation Climatology Centre V.2018	Monthly data based on interpolated gauges at 1.0º resolution	Schneider et al 2008
CRU: CRU TS 4.01 from the Climate Research Unit	Monthly data from interpolated gauges at 0.5º resolution	Harris et al 2020
CHIRPS: Climate Hazards Group InfraRed Precipitation with Station Data	Daily estimates from merged gauge and infrared satellite data, at 0.05º resolution	Funk et al 2015
ARC2: African Rainfall Climatology version 2	Daily estimates from merged gauge and infrared satellite data, at 0.1º resolution	Novella et al 2013
ERA5: European Centre for Medium-Range Weather Forecast Reanalysis	Daily reanalysis (output form a global circulation model, nudged by all available observations), at 0.1º resolution	Hersbach et al 2020
MSWEP: MSWEP v2.8 Mutli-Source Weighted-Ensemble Precipitation	3-hourly estimates from merged satellite, gauge, and reanalysis data, at 0.1º resolution	Beck et al 2019

Table 1: Details of the gridded rainfall observational products used for trend analysis

Figure 1a compares monthly rainfall trends over the period 1983-2016, common to all datasets. Data is first averaged over the area of HAD which exhibits a bimodal rainfall regime (Nicholson 2017). This area is shown by the black outline in Figure 1b, which shows the spatial variability in trends in seasonal and annual rainfall across HAD. For Figure 1b focuses in on CHIRPS and MSWEP to evaluate spatial aspects of the trend:

CHIRPS because it incorporates numerous gauge observations in Ethiopia and Somalia (where other gauge-based datasets have sparse coverage; Chris Funk, personal communication) and MSWEP as it incorporates reanalysis data and has shown to be one of the most accurate rainfall datasets in systematic global comparisons (Beck et al 2017).

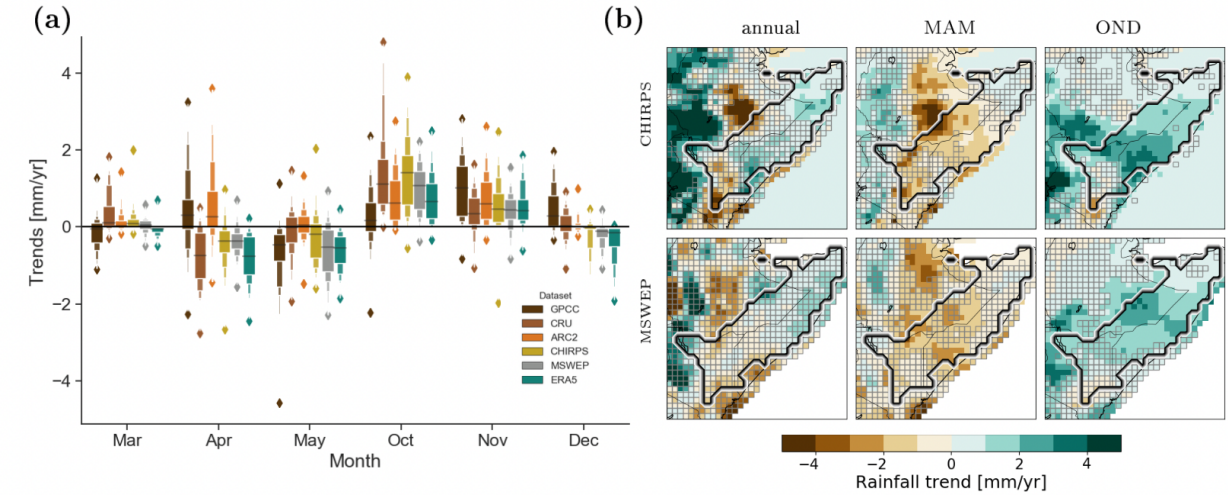

Figure 1 From Adloff et al, submitted. (a) Monthly rainfall trends within MAM (long rains) and OND (short rains) from six datasets. Each distribution represents the monthly rainfall trend across all pixels in the area framed black in panel (b). All trends are calculated over the period 1983-2016, depicted are the median and the 7th, 13th, 25th, 75th, 87th and 93rd percentiles. Diamonds represent outliers. (b) Linearly approximated time series trends in annual, MAM and OND rainfall in HAD. Grid cells with non-significant trends are framed in grey.

Results show broad agreement between rainfall datasets, showing negative MAM and positive OND rainfall trends over the period. The consistency between datasets based on different methodologies (including ERA5 which does not include any rain gauge data), demonstrates that trends are not an artefact of progressively decreasing numbers of rain gauges for the region, as has been previously suggested (Lorenz and Kunstmann, 2012, Maidment et al., 2015). The negative long rains trend appears mostly due to rainfall reductions in April and May, consistent with the documented trend of an earlier cessation of the long rains, although no decline in March rainfall is found, which might be expected given the suggestion of a later start to the season (Wainwright et al., 2019).

We next turn to the extreme rainfall component of seasonal totals, defined here using MSWEP data as the total of all 3-hourly periods within a season where rainfall is greater than the 95th percentile of 3-hourly rainfall. This is shown in Figure 2 for MAM and OND, where results are presented at a series of four locations, chosen to sample a transect across HAD. These four locations exhibit both positive and negative trends in extreme MAM rainfall, but only positive trends in extreme OND rainfall. We find a decline of 15mm in average MAM extreme rainfall contribution between 1980-1999 and 2000-2019 and an increase of 12mm in OND. Over the same period total seasonal rainfall declined by 23mm

for MAM and increased by 14mm for OND. This indicates that changes in extreme rainfall have been responsible for a significant part of changes in seasonal totals. Additionally, for both seasons the linear gradient of extreme rainfall trends is more positive than linear trends in seasonal rainfall totals, indicating a larger portion of rainfall falling in extreme events in the present day compared to the 1980s (Adloff et al., submitted).

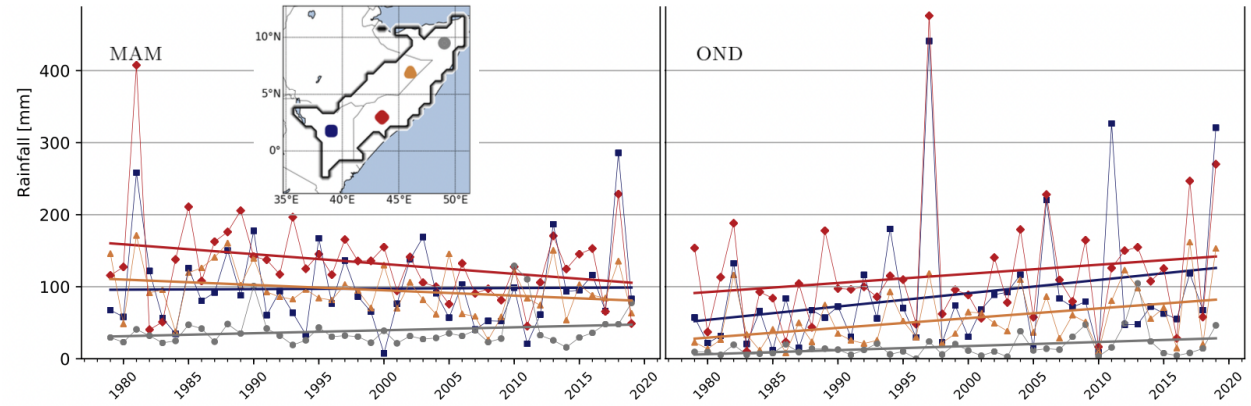

Figure 2 From Adloff et al., submitted. Time series of extreme seasonal rainfall total from MSWEP, 1979-2019 (falling in 3-hourly periods above the 95th percentile) in four locations across HAD (see inset map), along with the approximated linear trend line based on the Theil-Sen estimator (Theil, 1950; Sen, 1968). The data for each location are first averaged over a centralised area of 1.5°x1.5°.

3.2 Sources of HAD rainfall

To unravel the origins of the trends described above, we trace the terrestrial and oceanic moisture sources of long and short rains over HAD. Using this tracking methodology, we investigate changes in the contributions of ocean and land evaporation to HAD rainfall across the last four decades.

The water which causes rainfall in a specific region (termed 'sink region') will have last evaporated from local and/or remote land or ocean regions (termed 'source regions', or simply 'sources'). To identify the major sources of rainfall and quantify their relative contributions to local rainfall, we use the FLEXible PARTicle dispersion model (FLEXPART, Stohl et al. 2005), a Lagrangian atmospheric transport model. This simulates the trajectories of air parcels backward in time, i.e., from the sink region (HAD in this case) to the source regions (ocean or land). The model tracks the different properties of the air parcels such as temperature and water content as the parcel moves from the source to the sink region. The relative changes in the air parcel's water content can then be used to quantify the evaporation and rainfall occurring over a certain region. A negative change of an air parcel's water content is indicative of precipitation, whilst a positive change indicates evaporation over the region. With sufficient parcels, a reliable estimate of either precipitation or evaporation at any given point in time can be determined (Keune et al. 2021).

Here we use global simulations of the FLEXPART version 9.01, forced with the ERA-Interim reanalysis at 1° spatial resolution for the 37 years 1980–2016 (Dee et al. 2011). These FLEXPART simulations are based on approximately 2 million air parcels, uniformly distributed, and tracked in space and time. FLEXPART uses forcing information from several variables from ERA-Interim including horizontal and vertical 10-meter wind speed, temperature and specific humidity at multiple pressure levels including the surface, temperature and dew-point temperature at 2 meters, precipitation, sensible and latent heat fluxes: among others. Model output includes the properties of the air parcels at 3-hourly time steps, which are then post-processed using the Heat And MoiSture Tracking framEwoRk (HAMSTER v1.0.0) described by Keune et al. (2021). The precipitation and evaporation along the air parcel's trajectories are bias-corrected with satellite-based datasets and in-situ observations. Global Land Evaporation Amsterdam Model (GLEAM, Miralles et al. 2011, Martens et al. 2017) is used for land evaporation, Objectively Analyzed air-sea flux (OAFlux, Yu and Weller, 2007) is used for ocean evaporation, whilst CHIRPS is used as an estimate of rainfall (Funk et al. 2015). This setup provides an observation-constrained quantification and mapping of the sources of HAD's rainfall over time.

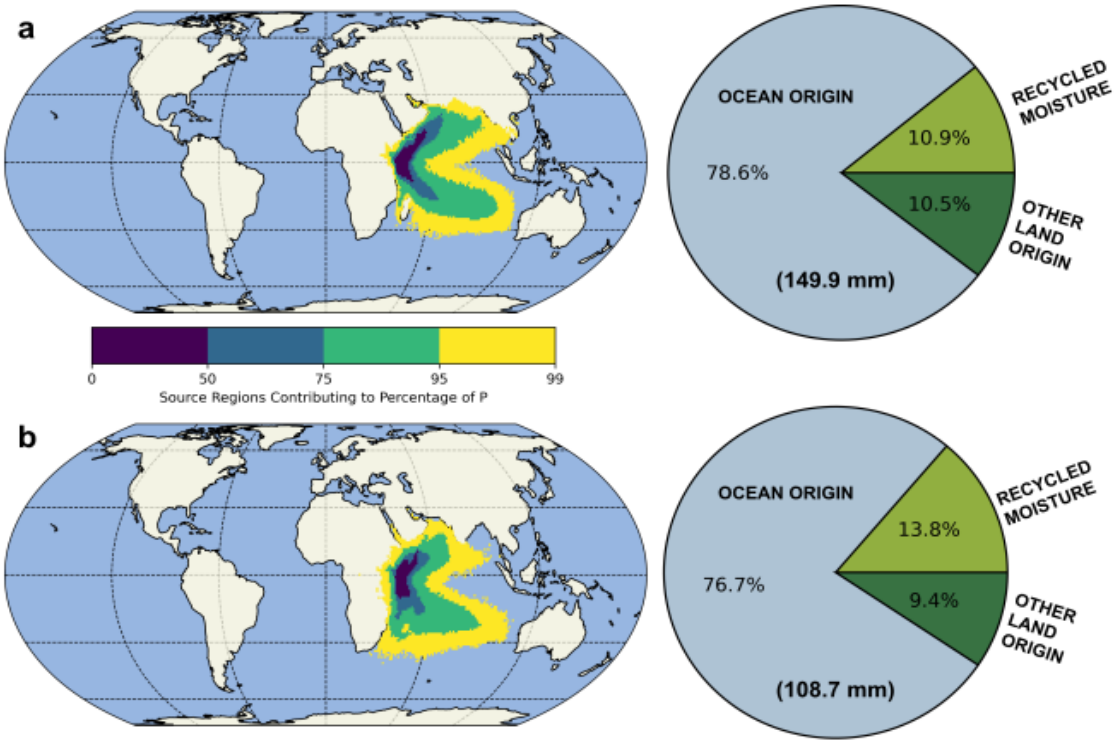

Figure 3 Sources of moisture contributing to HAD (a) long and (b) short rains, averaged over 1980-2016. For each season the map shows the source regions, and the pie chart shows the percent contribution to HAD precipitation of the ocean, HAD land area (recycled moisture), and land area outside the HAD (numbers in parentheses in the pie charts represent average seasonal precipitation).

Source regions are estimated for HAD (using the region defined in the analysis of section 3.1) and are shown for the long and short rains in Figure 3, based on long-term average contribution over 1980–2016. The colours (dark blue to yellow) represent the source regions which contribute to 0-50%, 50%-75%, 75%-90%, and 90%-99% of the average rainfall in the two seasons. Figure 3 also shows pie charts summarizing the relative contributions of ocean and land.

Around 80% of HAD rainfall originates from Indian Ocean evaporation, for both seasons. The source of long rains shows two distinct lobes of moisture sources: one extending from near the edge of the southern tropics to the HAD region and the other extending from the subtropics north of the equator. A similar pattern is seen in the oceanic source of the short rains, though with a smaller northern lobe of moisture source. These lobes likely arise from the intraseasonal evolution of Indian Ocean winds near HAD, which transition from northeasterlies to southeasterlies during the long rains, and vice versa in during the short rains. For both seasons the contribution of evaporation from land is relatively low compared to the ocean contribution. For the long rains, a similar amount of moisture originates from recycling (local) and from remote land sources (10.9% and 10.5% respectively), whilst the short rains shows a larger proportion of local recycling relative to remote land evaporation (13.8% compared to 9.4%). The larger contribution of remote land sources for the long rains can be seen in the source maps of Figure 3, which extends further over the Indian subcontinent and Southeast Asia for the long rains.

In this context of rainfall trends presented in the previous section (drier long rains and wetter short rains, with an increasing contribution of extreme rainfall) we evaluate trends in moisture sources based on the Lagrangian analysis above to scrutinise any possible changes in moisture source regions across the past few decades. This temporal variability is shown in Figure 4, for the three sources of moisture across both seasons. Ocean moisture is the dominant source in the long-term average shown in Figure 3, and this holds for all years individually. There is some interannual variability in the ocean contribution in both seasons; for the long rains it ranges from 67% (1981) to 87% (2000). The recycled moisture and moisture from other land sources are very similar to each other and each show a contribution of generally below 20% for each year across the period. We do note that the recycled contribution shows more variability compared to the contributions from the land outside HAD in the recent years (2008–onwards).

During the short rains, the recycled moisture is clearly the dominant land source, and reaches as high as 25% of the total rainfall (year 2011). Interestingly, we observe that the recycled moisture contribution as a percentage of the total short rains rainfall has increased in recent years (after 2010), with a corresponding reduction in the ocean contribution. This result shows the influence of the region's land surface on its own rainfall, indicating that land cover patterns and land use can influence precipitation in the region. This increase in precipitation is associated with a period of increased short rains rainfall. It may be that increased precipitation has simply increased moisture available for recycling, alternatively land cover changes have augmented local precipitation recycling,

driving increases in precipitation. It is not possible to determine causal relationships with the current analysis, but this is a question for future research.

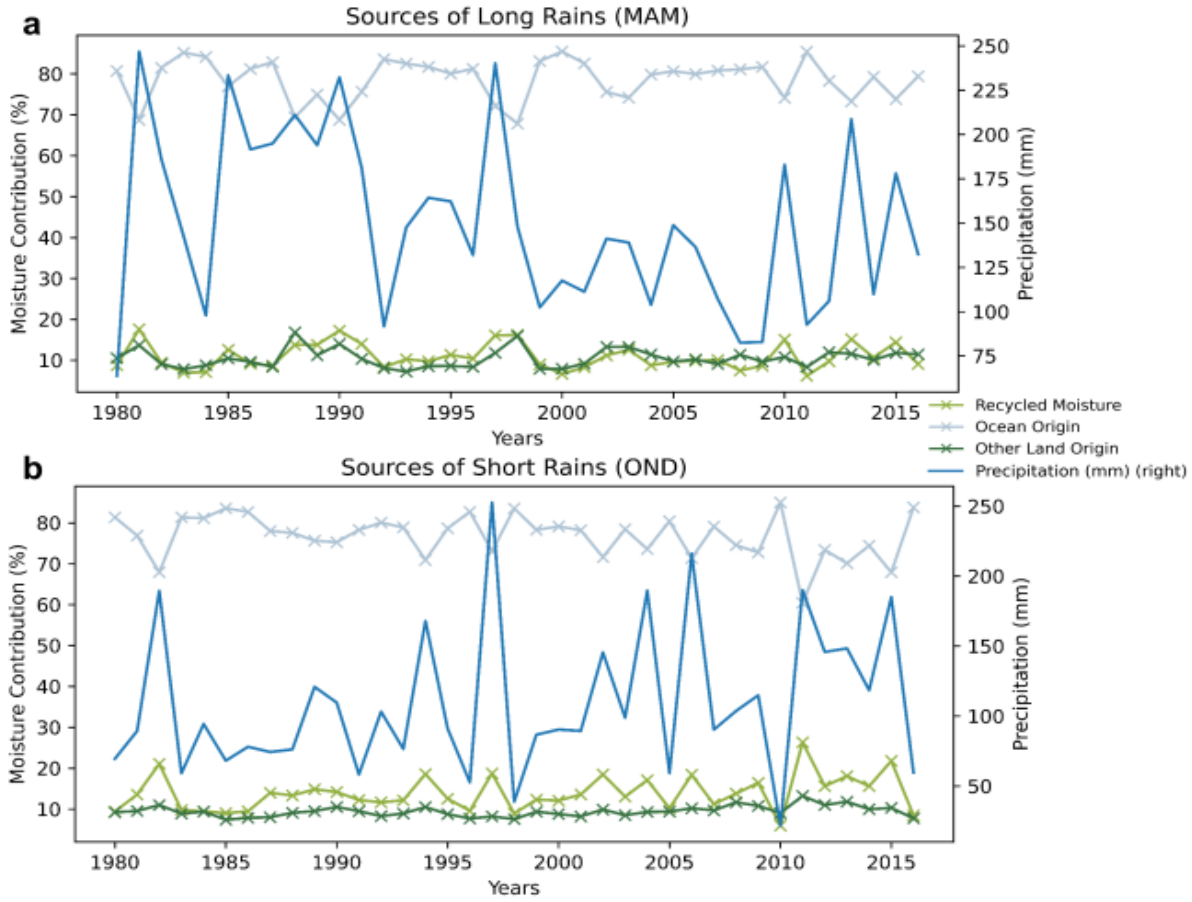

Figure 4. Time series of moisture contributions to the (a) long and (b) short rains over HAD. Precipitation totals are shown in dark blue (secondary axis).

In addition we note that seasons such as the short rains 2011 show an enhanced recycling component despite a reduction in contribution from the ocean. The land surface capacity for precipitation recycling may therefore help to stabilise seasonal rainfall totals during seasons when large scale climate conditions suppress moisture transport to HAD. Land cover changes which curb the potential for precipitation recycling may therefore threaten regional water security.

Recent findings illustrate the need to reconsider the idea of watersheds as isolated from one another, due to their dependency on moisture supplied by other watersheds through the atmosphere (Keune and Miralles, 2019). Our analysis indicates that a large fraction of the precipitation supply to the Horn of Africa has in fact an oceanic origin; yet at least 20% of the precipitation still originates over land, with 10% being generated outside the Horn of Africa region. Therefore, natural, or anthropogenic imbalances in the atmospheric trade from other watersheds may increase the pressure on local water resources in the

HAD region. Repercussions of upwind evaporation as a contributor to precipitation downwind should be considered in assessments of freshwater vulnerability. Likewise, droughts and water scarcity may also propagate from watershed to watershed due to the reduced evaporation associated with these events. This puts emphasis on the fact that freshwater availability and water use sustainability are global issues, and thus they know no political or geographical boundaries (Vörösmarty et al., 2015). Land and water management across watershed and region boundaries may help better understand the threats to water availability and security in the Horn of Africa region, and beyond.

There are several uncertainties associated with the Lagrangian analysis of HAD moisture sources presented here. First, the FLEXPART model is forced with ERA-Interim reanalysis data and as such the reliability of the FLEXPART output is influenced by the accuracy and consistency of the ERA-Interim output. In the future, new global runs of FLEXPART forced with the newer ERA5 reanalysis dataset could potentially reduce input-related errors. Second, the postprocessing of the FLEXPART-simulated trajectories is based on several assumptions including the nature of the atmospheric boundary layer (well-mixed), the humidity threshold at which the air parcels are assumed to rain out (relative humidity greater than 80%), the datasets used for bias correcting evaporation and precipitation along the parcel's trajectory (here GLEAM and ocean flux datasets are used for evaporation and CHIRPS is used for precipitation), among other factors.

In future work we will extend the analysis from the HAD region to two other climatologically distinct regions in the Horn of Africa: the Ethiopian highlands and the Kenyan highlands. In addition, the trends in the atmospheric sources of rainfall and their relationship with the ocean-atmosphere oscillations such as IOD, ENSO, and Madden-Julian Oscillation will be explored to develop new insights into the drivers of the short and long rains in the region. The FLEXPART simulations also enable the tracking of the transport of heat, and hence future research directions involve understanding the HAD heat waves from a Lagrangian perspective and exploring the coupling of heat and moisture transport in modulating the hydroclimate of the region.

3.3 Shifts in potential evapotranspiration and aridity in HAD

Potential evapotranspiration (PET) is a measure of atmospheric moisture demand, defined as the amount of evapotranspiration that would occur if sufficient water were available. PET is controlled by surface and air temperature, radiation, and wind speed. There are currently no available high-resolution datasets of PET. To address this, a new hourly PET dataset, hPET, has been produced as part of DOWN2EARTH, covering 1981-present (Singer et al., 2021). This has been generated by using the FAO Penman-Monteith equation with the state-of-the-art ERA5-Land reanalysis (https://cds.climate.copernicus.eu/cdsapp#!/dataset/reanalysis-era5-land?tab=overview). Using hPET we have evaluated historical changes in PET. PET also facilitates the calculation of aridity index (AI), defined as the ratio of precipitation to PET. We have also evaluated changes in AI, by combining CHIRPS annual precipitation with annual total PET.

To measure changes in precipitation, PET and AI, we calculate the most recent decadal average (2010-2019) and subtract the average of the first decade of the data (1981-1990). Figure 5 shows the change in the two components of AI: precipitation and PET, and the change in AI. Consistent with Figure 1, areas of increased rainfall can be seen across the Kenyan and Ethiopian highlands, and over the Kenya/Somalia border. In central/ southeast Ethiopia, southern Kenya, and coastal Somalia, declines in rainfall can be seen. PET changes are more homogenous, indicating increases everywhere, consistent with rising temperatures globally across the period (IPCC, 2021), although minimal changes in PET can be seen across the Ethiopian and Kenyan highlands. Relative to global trends in PET (not shown), we note that PET increases are particularly large over HAD.

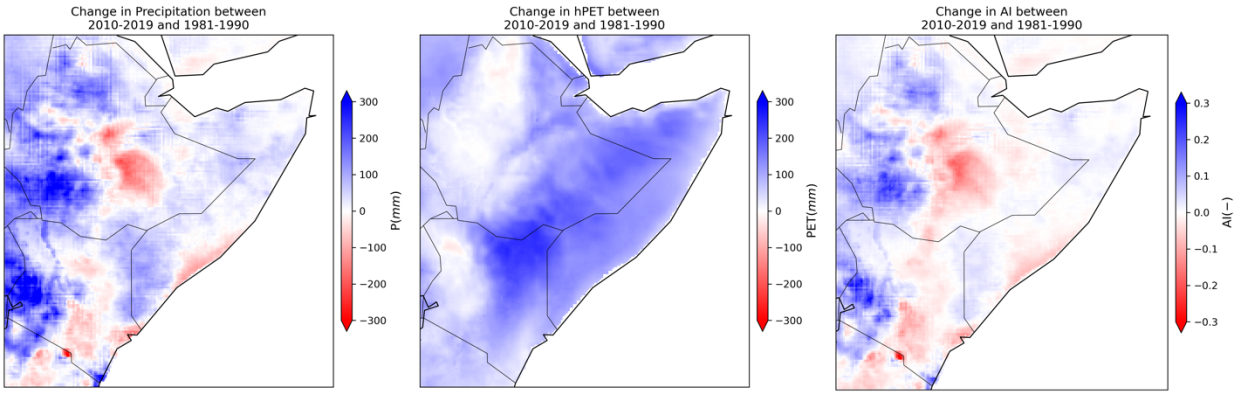

Figure 5: Change in CHIRPS annual precipitation total (left), hPET PET (middle) and AI calculated from the two (right), shown as the difference between the average of 2010-2019 and 1981-1990.

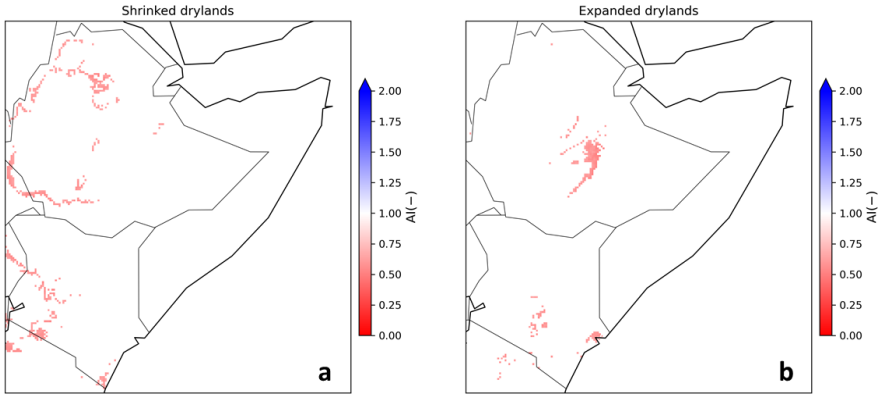

Figure 6: (a) Regions where changes in AI indicate shrinking drylands: where AI was below 0.65 in 1981-1990 but above 0.65 in 2010-2019 (b) Regions indicating expanding drylands: where AI was above 0.65 in 1981-1990 but dropped below 0.65 in 2010-2019.

Since AI is calculated as precipitation divided by PET, either lower precipitation or higher PET will lead to lower AI (increased aridity). This can be seen for HAD, where areas with lower precipitation and increased PET drive a decline in AI (corresponding to an increase in aridity): for central/southeast Ethiopia, southern Kenya, and coastal Somalia. Conversely, increased AI can be seen across the highlands of Ethiopia and Kenya due to increased rainfall without any significant change in PET.

Finally, we focus on the possible expansion or contraction of drylands (defined as an area with AI <0.65). Figure 6 shows regions where dryland areas are shrinking (AI increased from below to above 0.65 between 1981-1990 and 2010-2019, Figure 7a) or expanding (AI decreased from above to below 0.65, Figure 7b). Over HAD we find the largest expansion of drylands in central/southeast Ethiopia, along with some areas of southern Kenya. According to this analysis, the area of dryland appears to be shrinking around the perimeter of the Ethiopian Highlands, along with areas of the Kenyan highlands. Future development of this work will include a more detailed regional analysis, quantifying the relative role of precipitation and PET in driving AI changes, and studying the implication of existing changes on water availability by contrasting AI changes with changes in water balance components on a regional level.

4 Water indicators

4.1 Indices of drought

Trends in drought indices over HAD have been evaluated. The Standardized Precipitation Index (SPI) and the Standardized Precipitation-Evapotranspiration Index (SPEI) are commonly used as metrics of meteorological and agricultural drought respectively (Vicente-Serrano et al 2010). SPI measures the deviation of accumulated precipitation from its long-term range, whilst SPEI targets water balance at the surface, by measuring the deviation of precipitation minus PET and thus incorporating the impact of temperature variation. Both indices are defined as a continuous variable across time, with each value corresponding to anomalies across a specified temporal domain, such as 3, 6 or 12 months, with negative values indicating an increase in drought magnitude. Here we consider 12-month SPI and SPEI (SPI-12 and SPEI-12 hereafter), as a strong association has been demonstrated between these metrics and subsequent food insecurity (Coughlan de Perez et al., 2019). We focus on a threshold of -1, as the risk of food insecurity was shown to rise significantly following the exceedance of this threshold in pastoralist areas. In the following analysis precipitation is taken from MSWEP (Beck et al., 2019) and PET from hPET (Singer et al., 2021).

Figure 7 shows results for Kenya, Ethiopia, and Somalia, presenting the percentage of the country area affected by an SPI-12 or SPEI-12 drought below –1. Since 1981 there have been multiple sustained periods of long-term rainfall deficits (SPI-12) across all three countries. For Kenya the most severe rainfall deficit appears to be between 1999-2001, where SPI-12 remained below -1 for at least 30% of the country for two years. Severe droughts also occurred in 2009, 2011 and 2017. Meteorological drought also affected Ethiopia and Somalia at similar times to Kenya with the 2017 drought showing SPI-12 below -1 over 60% of each country, sustained for a year. This sustained period of poor rainfall led to a sixfold spike in the number of food-insecure people across the wider region (Funk, 2020).

The spatial footprint of recent meteorological droughts does not appear to be unprecedented in this analysis. Although SPI-12 dropped below -1 across 60% of Somalia in 2017, a similar duration of deficit can be seen in 1999, where the extent of the country experiencing drought conditions rose higher, to around 90%. In 1992 and 1984 SPI-12 dropped below -1 across 60% of the country, though these events did not last as long. Similarly, the spatial extent of the largest recent meteorological droughts affecting Ethiopia and Kenya is similar to drought events in the 1980s and 1990s.

However, an entirely different picture emerges when considering SPEI-12 as a proxy for available surface water (grey lines, Figure 7). SPEI incorporates the influence of atmospheric demand for water through inclusion of PET: higher PET leads to stronger “pull” of moisture to the atmosphere from the land surface, leading to a higher surface

water deficit given the same amount of rainfall. The previous section showed a trend toward higher PET in recent years, with a potential for exacerbation of SPEI drought.

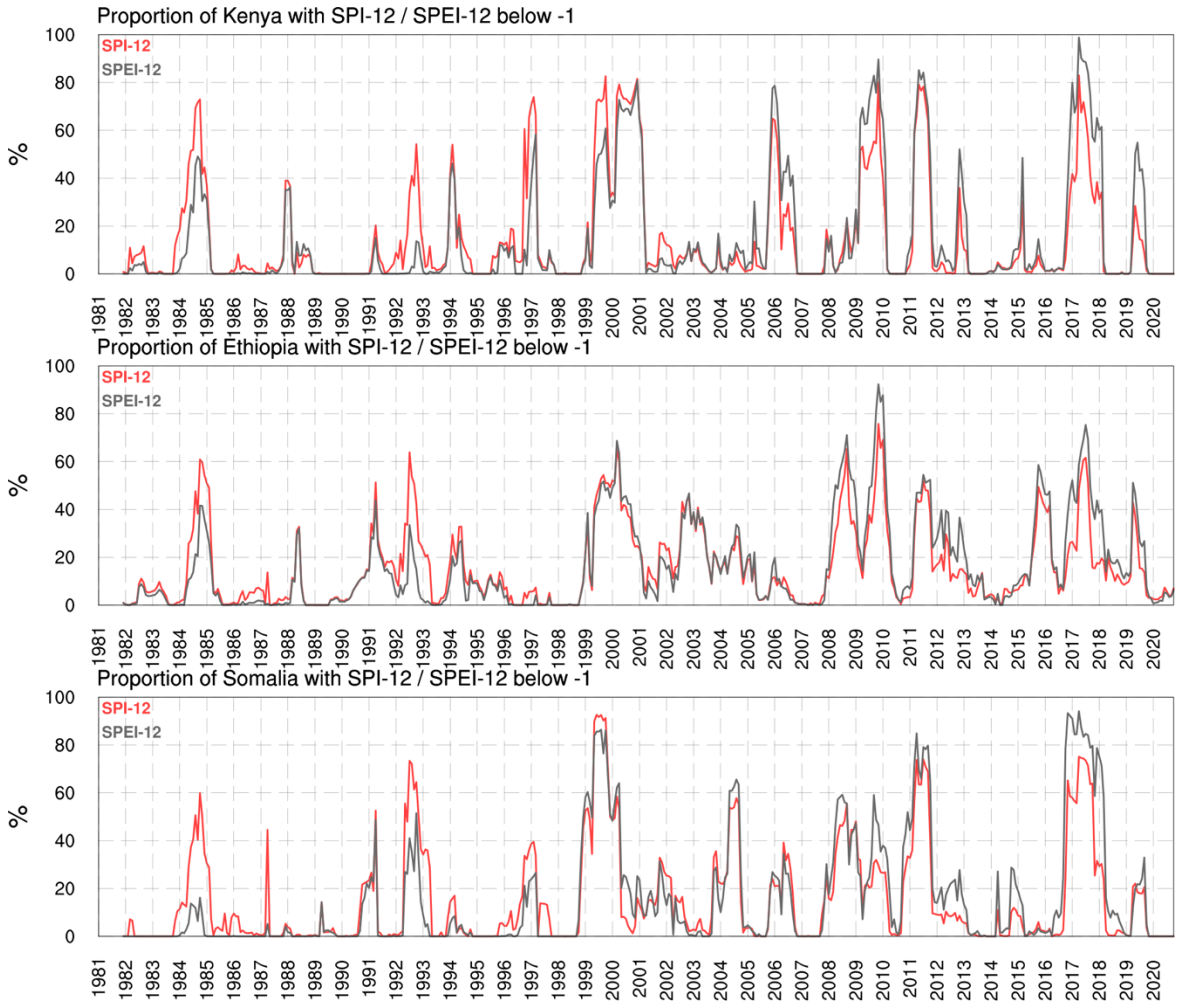

Figure 7 Historical record of SPI-12 and SPEI-12 (using MSWEP for precipitation and hPET for PET). For Kenya/Ethiopia/Somalia (top/middle/bottom) each plot shows the proportion of countries showing a value below a threshold of -1. Red line shows SPI-12 grey shows SPEI-12. Location of data along the x-axis corresponds to the 12-month period up to that point (e.g., data aligned with "1982" represents the conditions in the 12 months up to the start of 1982).

A trend toward more extensive and sustained SPEI-12 drought is shown clearly in Figure 7. Before 1999 SPEI-12 dropped below -1 across more than 40% of the country infrequently: three times for Kenya, twice for Ethiopia and twice for Somalia, and in each case the spatial extent of the drought did not persist beyond a few months. By contrast events with a similar spatial extent have not only become more common in recent years (occurring eight times in Kenya since 1999 for instance) but have become much more sustained when they do occur: SPEI-12 remained below -1 for at least 40% of the country in 2017, with conditions persisting for over a year. Recent years have also seen an

unprecedented spatial scale of SPEI-12 drought. Before 1999 the highest spatial extent of SPEI-12 below -1 was around 40% for each country. In the sustained 1999 event this record was broken in Ethiopia, reaching 60% briefly. A similar event was seen in 2008, evolving into another record-breaking event the following year where the drought affected over 80% of the country. Higher proportions of the area of Kenya and Somalia have been affected in recent years: the 1999 event broke the SPEI-12 record for spatial extent, reaching 80% in both countries. An 80% affected area was seen again in 2006, 2009 and 2011 in Kenya, and in 2011 in Somalia. The most recent drought in 2017 broke the record again for both countries, where over 90% of Somalia remained below SPEI-12 for multiple months, and over Kenya the start of 2017 saw a brief period where 100% of the country faced SPEI-12 conditions below -1.

4.2 Water storage

To understand changes in HAD subsurface water storage, we calculated trends in total water storage (TWS) from GRACE. We used the latest release of the monthly GRACE L2 product provided by the Center for Space Research (CSR Release-06), covering April 2002 to January 2020, expressed as dimensionless spherical harmonic coefficients up to degree and order 96. To generate monthly TWS changes from the GRACE product, degree 1 and zonal degree 2 spherical harmonic coefficients were replaced by those from Swenson et al. (2008) and zonal degree 2 coefficients from Satellite Laser Ranging data (Chen et al., 2007), respectively. Correlated errors were minimized through the application of the DDK2 anisotropic decorrelation filter (Kusche et al., 2009). Full details of the processing of GRACE data will be found in Adloff et al, submitted.

During the period of GRACE TWS (2002-2020), East Africa did not experience mass changes related to glacial isostatic adjustments nor are we aware of notable changes in biomass. Therefore, we assume that recorded mass anomalies predominantly reflect the hydrological cycle. Since our focus is on dryland areas, we further assume that surficial water and soil moisture are minimal, so that TWS anomalies measured in dry months following rainy seasons predominantly reflect changes in soil moisture (below the evaporation zone) due to deep infiltration and groundwater storage resulting from groundwater recharge.

TWS trends across HAD are shown in Figure 8a, with Figure 8b showing the estimated contributions from each rainfall season for four points in a transect across the region. These contributions are estimated by calculating the difference in TWS across each season (ΔTWS) and averaging over all years. Over the GRACE period (2003-2016), TWS shows a positive trend of ~4 mm/yr. This suggests that despite increasing droughts and failing MAM rains (Figure 1; Funk et al., 2020), subsurface water storage has not declined, and is in fact rising across HAD. This increase in TWS is most evident in inland areas of Kenya and in Ethiopia. The short record and high interannual variability preclude statistical significance of these rising TWS trends. Nevertheless, analysis does not show a significant negative TWS trend. This indicates that TWS is stable in the face of higher PET and declining long rains. For northern Kenya and southern Somalia (locations A and

B), we find that the annual TWS storage trends are comprised of positive ΔTWS from both seasons, while for Somaliland (location D), the negative ΔTWS_{MAM} trend is offset by a strongly positive ΔTWS_{OND} trend, producing an overall positive annual trend in TWS. In contrast, the positive ΔTWS_{MAM} trend compensates for the small negative ΔTWS_{OND} trend in eastern Ethiopia (location C), leading to an overall positive trend in annual TWS.

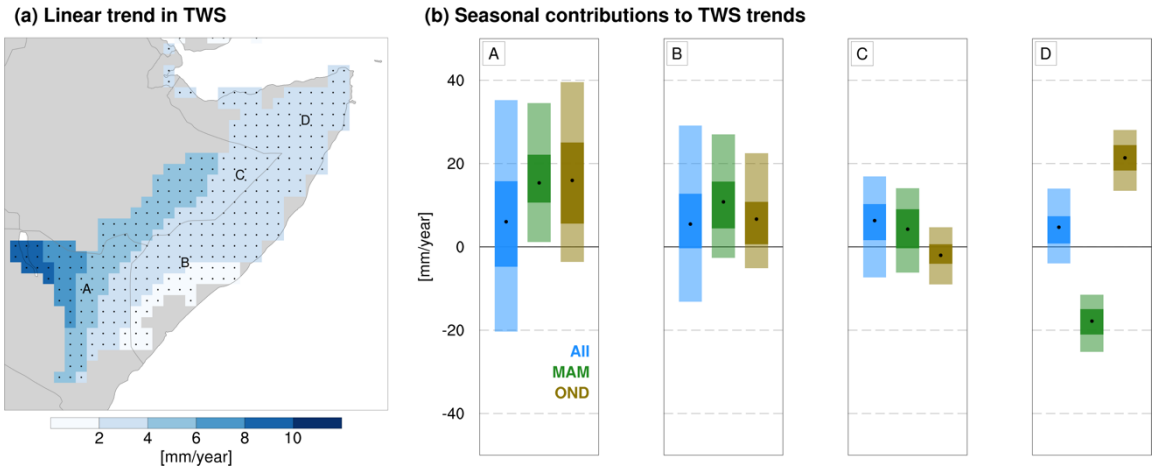

Figure 8: From Adloff et al, submitted. (a) Trends in monthly TWS over the period 2003-2016; stippling is applied at pixels where bootstrapping indicates the trend is not significantly different from zero. (b) Bootstrapped overall trend and seasonal contributions to the TWS trend for the four locations indicated in (a). This subplot shows the overall linear trend in monthly TWS (All), and the contributions from long rains (MAM) and short rains (OND), based on accumulated ΔTWS for each season; outer and inner box boundaries represent the 5th-95th and 25th-75th percentiles of the bootstrapped trend contribution estimates and the central dot indicates the median value.

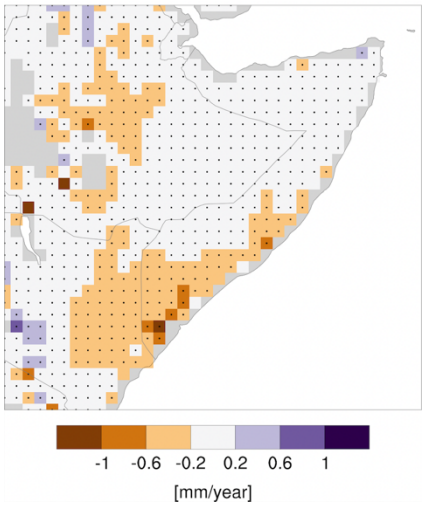

Figure 9: From Adloff et al, submitted. Trend in annual soil moisture based on Passive ESA CCI, 2003-2016

To clarify the origin of TWS trends we also analyse monthly soil moisture from satellite estimates: Passive ESA CCI (https://www.esa-soilmoisture-cci.org/). We converted the soil water content to mm using a length scale of 10 cm enabling direct comparison with TWS. Trends in annual soil moisture across the GRACE period 2003-2016 are shown in Figure 9. Results show negative trends over the southern Somalia and Kenya coasts and in parts of the Ethiopian highlands. No trends are above statistical significance, however. Trends calculated across each month individually (not shown) indicate no decline during “wet” months, with all declines occurring during dry months, suggesting increased PET as a driver of soil moisture declines rather than reduced rainfall.

In context with the increasing TWS trend, the result that soil moisture has declined slightly across the period suggests that increasing TWS cannot be accounted for by a change in near-surface soil moisture. We infer then that the rise in TWS must be associated with subsurface water storage, where water has percolated past the root zone. In a region where vegetation is sparse (i.e., where transpiration is not the dominant driver of moisture return to the atmosphere), we conclude that this incline in TWS represents an increase in sub-surface water, on its way to be stored long-term as groundwater.

5 Summary

Analysis presented in this report indicates a decline in long rains, consistent with previous literature. The decline in the long rains and more frequent drought events has been linked to anthropogenic ocean warming in the Pacific (Funk et al., 2019): continued global warming suggests this trend will continue. However, model projections for the 21st century for the long rains point to increased rainfall. This so-called East Africa Climate Paradox has not been entirely resolved and the future direction of long rains total rainfall is uncertain. Results presented here show a consistent decline in April and May rainfall across observational rainfall datasets. No decline in March rainfall is found, which is somewhat inconsistent with the suggestion that the long rains decline is due to a trend toward later rainfall onset (Wainwright et al., 2019).

A trend toward increased short rains rainfall is found across all observational datasets, arising from increased totals in October and November. This is consistent with previous work from Gebrechorkos et al. (2019) which found an increase in OND totals, but generally below statistical significance. A lack of statistical significance may arise from considering the season in its entirety: our results indicate no strong trend in December rainfall which may obscure the trend arising from the other two months of the season. Results shown here also indicate an increased frequency of the extreme rainfall component of the short rains, which is anticipated as a warming atmosphere can hold more moisture (IPCC, 2021).

We also show a clear trend toward higher PET across HAD, likely driven by higher near-surface air temperatures. This higher PET has led to increases in aridity over the past 40 years. Analysis indicates that part of central/southern Ethiopia (in Oromia region) appears to have recently moved into dryland range (AI < 0.65), along with parts of southern Kenya. Increased PET has also driven record-breaking droughts, as measured by the Standardized Precipitation Evapotranspiration Index, with spatial extent and duration of significant drought events reaching unprecedented levels in recent years. We also find a decline in near-surface soil moisture in dry months, likely driven by PET changes.

In contrast to increasing drought frequency, we find a positive trend in water storage below the root zone. The length of available data (14 years) limits the statistical power of trend analysis, but analysis indicates that this storage component has not experienced a notable decline in response to the long rains decline since 2000. The (non-significant) increase in water storage is consistent with the increase in extreme rainfall contribution to seasonal total rainfall, due to the dominant contribution of extreme rainfall to groundwater recharge (Taylor et al., 2013).

In summary, recent years have seen increases in drought frequency, magnitude, and extent, driven by declining long rains and temperature-driven PET increases. Simultaneously, increases in extreme rainfall particularly in the short rains have occurred. These increasing extremes are likely driving flooding (not shown) but may also be augmenting groundwater storage through the process of focussed recharge in dryland

ephemeral river channels. Increasing groundwater abstraction has the potential to buffer the impact of increasing drought frequency and any future increases in extreme rainfall are likely to further bolster this critical resource.

References

Adloff, M., Singer M.B., MacLeod, D.A, Michaelides, K., Mehrnegar, N., Hansford, E., Funk, C. and Mitchell, D. Sustained water storage in Horn of Africa drylands dominated by seasonal rainfall extremes, *in review at Environmental Research Letters.*

Amou, M., Gyilbag, A., Demelash, T. and Xu, Y., 2021. Heatwaves in Kenya 1987–2016: Facts from CHIRTS High Resolution Satellite Remotely Sensed and Station Blended Temperature Dataset. *Atmosphere*, *12*(1), p.37.

Beck, H.E., Vergopolan, N., Pan, M., Levizzani, V., Van Dijk, A.I., Weedon, G.P., Brocca, L., Pappenberger, F., Huffman, G.J. and Wood, E.F., 2017. Global-scale evaluation of 22 precipitation datasets using gauge observations and hydrological modeling. *Hydrology and Earth System Sciences*, *21*(12), pp.6201-6217.

Beck, H.E., Zimmermann, N.E., McVicar, T.R., Vergopolan, N., Berg, A. and Wood, E.F., 2018. Present and future Köppen-Geiger climate classification maps at 1-km resolution. *Scientific data*, *5*(1), pp.1-12.

Beck, H.E., Wood, E.F., Pan, M., Fisher, C.K., Miralles, D.G., Van Dijk, A.I., McVicar, T.R. and Adler, R.F., 2019. MSWEP V2 global 3-hourly 0.1 precipitation: methodology and quantitative assessment. *Bulletin of the American Meteorological Society*, *100*(3), pp.473-500.

Camberlin, P., 2017. Temperature trends and variability in the Greater Horn of Africa: interactions with precipitation. *Climate Dynamics*, *48*(1-2), pp.477-498.

de Perez, E.C., van Aalst, M., Choularton, R., van den Hurk, B., Mason, S., Nissan, H. and Schwager, S., 2019. From rain to famine: assessing the utility of rainfall observations and seasonal forecasts to anticipate food insecurity in East Africa. *Food security*, *11*(1), pp.57-68.

Dee, D. P., Uppala, S. M., Simmons, A. J., Berrisford, P., Poli, P. et al.: The ERA-Interim reanalysis: Configuration and performance of the data assimilation system, Q. J. Roy. Meteor. Soc., 137(656), 553–597, 2011.

Funk, C., 2020. Ethiopia, Somalia and Kenya face devastating drought. *Nature*, *586*(7831), pp.645-646.

Funk 2021, Drought Flood Fire, Cambridge University Press

Funk, C., Peterson, P., Landsfeld, M., Pedreros, D., Verdin, J., Shukla, S., Husak, G., Rowland, J., Harrison, L., Hoell, A. and Michaelsen, J., 2015. The climate hazards infrared precipitation with stations—a new environmental record for monitoring extremes. *Scientific data*, *2*(1), pp.1-21.

Funk, C., Pedreros, D., Nicholson, S., Hoell, A., Korecha, D., Galu, G., Artan, G., Segele, Z., Tadege, A., Atheru, Z. and Teshome, F., 2019. Examining the potential contributions of extreme “Western V” sea surface temperatures to the 2017 March–June East African drought. *Bulletin of the American Meteorological Society*, *100*(1), pp.S55-S60.

Gebrechorkos, S.H., Hülsmann, S. and Bernhofer, C., 2019. Long-term trends in rainfall and temperature using high-resolution climate datasets in East Africa. *Scientific reports*, *9*(1), pp.1-9.

Haile, G.G., Tang, Q., Leng, G., Jia, G., Wang, J., Cai, D., Sun, S., Baniya, B. and Zhang, Q., 2020. Long-term spatiotemporal variation of drought patterns over the Greater Horn of Africa. *Science of the Total Environment*, *704*, p.135299.

Harris, I., Osborn, T.J., Jones, P. and Lister, D., 2020. Version 4 of the CRU TS monthly high-resolution gridded multivariate climate dataset. *Scientific data*, *7*(1), pp.1-18.

Hersbach, H., Bell, B., Berrisford, P., Hirahara, S., Horányi, A., Muñoz-Sabater, J., Nicolas, J., Peubey, C., Radu, R., Schepers, D. and Simmons, A., 2020. The ERA5 global reanalysis. *Quarterly Journal of the Royal Meteorological Society*, *146*(730), pp.1999-2049.

IPCC, 2021: Climate Change 2021: The Physical Science Basis. Contribution of Working Group I to the Sixth Assessment Report of the Intergovernmental Panel on Climate Change [Masson-Delmotte, V., P. Zhai, A. Pirani, S.L. Connors, C. Péan, S. Berger, N. Caud, Y. Chen, L. Goldfarb, M.I. Gomis, M. Huang, K. Leitzell, E. Lonnoy, J.B.R. Matthews, T.K. Maycock, T. Waterfield, O. Yelekçi, R. Yu, and B. Zhou (eds.)]. Cambridge University Press. In Press.

Keune, J., & Miralles, D. G. (2019). A precipitation recycling network to assess freshwater vulnerability: Challenging the watershed convention. Water Resources Research, 55, 9947– 9961. https://doi.org/10.1029/2019WR025310

Keune, J., Schumacher, D. L., and Miralles, D. G.: A holistic framework to estimate the origins of atmospheric moisture and heat using a Lagrangian model, Geosci. Model Dev. Discuss. [preprint], in review, 2021.

Kilavi, M., MacLeod, D., Ambani, M., Robbins, J., Dankers, R., Graham, R., Titley, H., Salih, A.A. and Todd, M.C., 2018. Extreme rainfall and flooding over central Kenya including Nairobi city during the long-rains season 2018: causes, predictability, and potential for early warning and actions. *Atmosphere*, *9*(12), p.472.

Lorenz, C., & Kunstmann, H. (2012). The hydrological cycle in three state-of-the-art reanalyses: Intercomparison and performance analysis. *Journal of Hydrometeorology*, *13*(5), 1397-1420.

MacLeod, D., Graham, R., O'Reilly, C., Otieno, G. and Todd, M., 2021. Causal pathways linking different flavours of ENSO with the Greater Horn of Africa short rains. *Atmospheric Science Letters*, *22*(2), p.e1015.

Maidment, R.I., Allan, R.P. and Black, E., 2015. Recent observed and simulated changes in precipitation over Africa. *Geophysical Research Letters*, *42*(19), pp.8155-8164.

Martens, B., Miralles, D. G., Lievens, H., Van Der Schalie, R., De Jeu, R. A., Fernández-Prieto, D., Beck, H., Dorigo, W., & Verhoest, N. E. (2017). GLEAM v3: Satellite-based land evaporation and root-zone soil moisture. Geosci. Model Dev., 10(5), 1903-1925.

Miralles, D. G., Holmes, T. R. H., De Jeu, R. A. M., Gash, J. H., Meesters, A. G. C. A., & Dolman, A. J. Global land-surface evaporation estimated from satellite-based observations. Hydrology and Earth System Sciences, 15(2), 453-469, 2011.

Nicholson, S.E., 2017. Climate and climatic variability of rainfall over eastern Africa. *Reviews of Geophysics*, *55*(3), pp.590-635.

Nicholson, S.E., Fink, A.H., Funk, C., Klotter, D.A. and Satheesh, A.R., 2021. Meteorological causes of the catastrophic rains of October/November 2019 in equatorial Africa. *Global and Planetary Change*, p.103687.

Novella, N.S. and Thiaw, W.M., 2013. African rainfall climatology version 2 for famine early warning systems. *Journal of Applied meteorology and Climatology*, *52*(3), pp.588-606.

Onyutha, C., 2021. Trends and variability of temperature and evaporation over the African continent: Relationships with precipitation. *Atmósfera*, *34*(3), pp.267-287.

Rowell, D.P., Booth, B.B., Nicholson, S.E. and Good, P., 2015. Reconciling past and future rainfall trends over East Africa. *Journal of Climate*, *28*(24), pp.9768-9788.

Schneider, U., Fuchs, T., Meyer-Christoffer, A. and Rudolf, B., 2008. Global precipitation analysis products of the GPCC. *Global Precipitation Climatology Centre (GPCC), DWD, Internet Publikation*, *112*.

Sen, P. K. (1968). Estimates of the regression coefficient based on Kendall's tau. American Statistical Association Journal 63, 1379–1389.

Singer, M.B., Asfaw, D.T., Rosolem, R., Cuthbert, M.O., Miralles, D.G., MacLeod, D., Quichimbo, E.A. and Michaelides, K., 2021. Hourly potential evapotranspiration at 0.1° resolution for the global land surface from 1981-present. *Scientific Data*, *8*(1), pp.1-13.

Stagge, J.H., Tallaksen, L.M., Gudmundsson, L., Van Loon, A.F. and Stahl, K., 2015. Candidate distributions for climatological drought indices (SPI and SPEI). *International Journal of Climatology*, *35*(13), pp.4027-4040.

Stohl, A., Forster, C., Frank, A., Seibert, P. and Wotawa, G., 2005. The Lagrangian particle dispersion model FLEXPART version 6.2. *Atmospheric Chemistry and Physics*, *5*(9), pp.2461-2474.

Taylor, R.G., Todd, M.C., Kongola, L., Maurice, L., Nahozya, E., Sanga, H. and MacDonald, A.M., 2013. Evidence of the dependence of groundwater resources on extreme rainfall in East Africa. *Nature Climate Change*, *3*(4), pp.374-378.

Theil, H. (1950). A rank-invariant method of linear and polynomial regression analysis, III. Proceedings of the Koninklijke Nederlandse Akademie van Wetenschappen A, 53, 1397–1412.

Vicente-Serrano, S.M., Beguería, S. and López-Moreno, J.I., 2010. A multiscalar drought index sensitive to global warming: the standardized precipitation evapotranspiration index. Journal of climate, 23(7), pp.1696-1718.

Vörösmarty, C.J., Hoekstra, A.Y., Bunn, S.E., Conway, D. and Gupta, J., 2015. What scale for water governance. Science, 349(6247), pp.478-479.

Wainwright, C.M., Marsham, J.H., Keane, R.J., Rowell, D.P., Finney, D.L., Black, E. and Allan, R.P., 2019. 'Eastern African Paradox'rainfall decline due to shorter not less intense Long Rains. *npj Climate and Atmospheric Science*, *2*(1), pp.1-9.

Yang, W., Seager, R., Cane, M.A. and Lyon, B., 2015. The annual cycle of East African precipitation. *Journal of Climate*, *28*(6), pp.2385-2404.

Yu, L., & Weller, R. A. Objectively analyzed air–sea heat fluxes for the global ice-free oceans (1981–2005). Bulletin of the American Meteorological Society, 88(4), 527-540, 2007.

Appendix 1: Abstract of Adloff et al, submitted

Sustained water storage in Horn of Africa drylands dominated by seasonal rainfall extremes

Submitted to Environmental Research Letters, November 2021

Markus Adloff[1], Michael Bliss Singer[2,3,4], David A. MacLeod[1], Katerina Michaelides[1,4,5], Nooshin Mehrnegar[2], Eleanor Hansford[1,&], Chris Funk[6], Daniel Mitchell[1,5]

[1]School of Geographical Sciences, University of Bristol, Bristol, United Kingdom
[2] School of Earth and Environmental Sciences, Cardiff University, Cardiff, United Kingdom
[3] Water Research Institute, Cardiff University, Cardiff, United Kingdom
[4] Earth Research Institute, University of California Santa Barbara, Santa Barbara, USA
[5] Cabot Institute for the Environment, University of Bristol, Bristol, United Kingdom
[6] University of California, Santa Barbara Climate Hazards Center, Santa Barbara, USA
[&] Now at European Centre for Medium-Range Weather Forecasts (ECMWF), Reading, United Kingdom

Abstract

Rural communities in the Horn of Africa Drylands (HAD) are increasingly vulnerable to multi-season droughts due to the strong dependence of livelihoods on seasonal rainfall. Recent declines of March-April-May rainfall have decreased available soil moisture, leading to crop losses and livestock death, and raising questions about the sustainability of water resources in the region. Here, we analyse multiple observational rainfall products for decadal trends in mean and extreme seasonal rainfall, as well as satellite-derived terrestrial water storage trends and patterns arising from two key rainfall seasons across various subregions of HAD from the beginning of the 21st century. We show that, despite decreases in March-April-May rainfall, total water storage in the HAD has not declined. In fact, our evidence points to an increasing trend in total water storage, which is largely associated with deep infiltration and groundwater recharge, and correlates strongly with total rainfall in the two dominant rainfall seasons over recent decades, and especially with extreme rainfall. We further show that high-intensity October-November-December rainfall associated with positive Indian Ocean Dipole events lead to the largest seasonal increases in water storage that persist over multiple years. These findings suggest that developing groundwater resources in HAD could offset or mitigate the impacts of increasingly common droughts, and thus form a key component to building resilience to the impacts of climate variability and climate change.

Appendix 2: Abstract of Singer et al 2021

Hourly potential evapotranspiration at 0.1° resolution for the global land surface from 1981-present

Michael Bliss Singer[1,2,3], Dagmawi Teklu Asfaw[4], Rafael Rosolem[5,6], MarkO.Cuthbert[1,7], Diego G. Miralles[8] , David MacLeod[4] , Edisson Andrés Quichimbo[1] & Katerina Michaelides[3,4,6]

[1]School of Earth and Environmental Sciences, Cardiff University, Cardiff, CF10 3AT, United Kingdom.
[2]Water Research Institute, Cardif University, Cardif, CF10 3AX, United Kingdom.
[3] Earth Research Institute, University of California Santa Barbara, Santa Barbara, CA, 93106, USA.
[4] School of Geographical Sciences, University of Bristol, Bristol, BS8 1SS, United Kingdom.
[5] Department of Civil Engineering, University of Bristol, BS8 1TR, Bristol, United Kingdom.
[6] Cabot Institute for the Environment, University of Bristol, Bristol, BS8 1QU, United Kingdom.
[7] School of Civil and Environmental Engineering, The University of New South Wales (UNSW), Sydney, Australia.
[8] Hydro-Climate Extremes Lab (H-CEL), Ghent University, Ghent, 9000, Belgium.

Published in *Scientific Data*

Abstract

Challenges exist for assessing the impacts of climate and climate change on the hydrological cycle on local and regional scales, and in turn on water resources, food, energy, and natural hazards. Potential evapotranspiration (PET) represents atmospheric demand for water, which is required at high spatial and temporal resolutions to compute actual evapotranspiration and thus close the water balance near the land surface for many such applications, but there are currently no available high-resolution datasets of PET. Here we develop an hourly PET dataset (hPET) for the global land surface at 0.1° spatial resolution, based on output from the recently developed ERA5-Land reanalysis dataset, over the period 1981 to present. We show how hPET compares to other available global PET datasets, over common spatiotemporal resolutions and time frames, with respect to spatial patterns of climatology and seasonal variations for selected humid and arid locations across the globe. We provide the data for users to employ for multiple applications to explore diurnal and seasonal variations in evaporative demand for water.

Appendix 3: Abstract of Keune et al. 2021

A holistic framework to estimate the origins of atmospheric moisture and heat using a Lagrangian model

Jessica Keune, Dominik L. Schumacher, and Diego G. Miralles

Hydro-Climate Extremes Lab (H-CEL), Ghent University, Ghent, 9000, Belgium.

Published in *Geoscientific Model Development Discussions*

Abstract
Despite the existing myriad of tools and models to assess atmospheric source–receptor relationships, their uncertainties remain largely unexplored and arguably stem from the scarcity of observations available for validation. Yet, Lagrangian models are increasingly used to determine the origin of precipitation and atmospheric heat, scrutinizing the changes in moisture and temperature along air parcel trajectories. Here, we present a holistic framework for the process-based evaluation of atmospheric trajectories to infer source–receptor relationships of both moisture and heat. The framework comprises three steps: (i) the diagnosis of moisture and heat from Lagrangian trajectories using multi-objective criteria to evaluate the accuracy and reliability of the fluxes, (ii) the attribution of sources following mass- and energy-conserving algorithms in order to establish source–receptor relationships, and (iii) the bias correction of diagnosed fluxes and the corresponding source–receptor relationships. Applying this framework to simulations from the Lagrangian model FLEXPART, driven with ERA-Interim reanalysis data, allows us to quantify the errors and uncertainties associated with the resulting source–receptor relationships for three cities in different climates (Beijing, Denver and Windhoek). Our results reveal large uncertainties inherent in the estimation of heat and precipitation origin with Lagrangian models, but they also demonstrate the synergistic impacts of source- and sink bias-corrections. The proposed framework paves the way for a cohesive assessment of the dependencies in source–receptor relationships.

Citation: *Keune, J., Schumacher, D.L. and Miralles, D.G., 2021. A holistic framework to estimate the origins of atmospheric moisture and heat using a Lagrangian model. Geoscientific Model Development Discussions, pp.1-33.*